Fluorescence lifetime measurements of molecular rotors for protein solubility prediction through non-specific interactions characterization

Yevgeniya Karibjanova, Isaac Rodríguez-Ruiz, Angel Orte, José Antonio Gavira, Pierre Roblin, Sébastien Teychené, Sébastien Teychené

Journal of Molecular Liquids 415 (2024) 126350

Contents lists available at ScienceDirect

Journal of Molecular Liquids

journal homepage: www.elsevier.com/locate/molliq

Fluorescence lifetime measurements of molecular rotors for protein solubility prediction through non-specific interactions characterization

Yevgeniya Karibjanova [a], Isaac Rodriguez-Ruiz [a,*], Angel Orte [b], José Antonio Gavira [c], Pierre Roblin [a], Sébastien Teychené [a]

[a] Laboratoire de Génie Chimique, CNRS, INP, UPS, Toulouse, France
[b] Nanoscopy-UGR Laboratory, Departamento de Fisicoquimica, Facultad de Farmacia, UGR, Granada, Spain
[c] Laboratory for Crystallographic Studies, LEC, IACT, CSIC, Granada, Spain

A B S T R A C T

Accurate characterization of protein–protein interactions is essential for understanding and controlling protein crystallization and phase transitions in a wide range of multidisciplinary fields, from fundamental and materials research to various pharma and industrial applications. This study introduces an innovative use of Fluorescence Lifetime Imaging Microscopy (FLIM) with the non-conjugated molecular rotor Sulforhodamine-B (SRB) for the characterization and comprehension of protein interactions, offering a new, efficient method for screening protein phase transition conditions. As models of study, non-specific intermolecular interactions in Lysozyme and Bovine Serum Albumin (BSA) solutions were investigated under various precipitant agents (salts, polymers) and pH conditions. FLIM analyses reveal a strong correlation between SRB fluorescence lifetime and the transition from repulsive to attractive protein interaction state, with a pronounced increase of the lifetime around the solubility point, enabling robust qualitative solubility predictions. Complementary SAXS analysis confirms that SRB acts uniquely as a probe for protein interactions without influencing the system state. Further time-resolved FLIM analysis on SRB lifetime populations indicates that the sensitivity of the fluorescence lifetime to protein interactions is driven by variation in probe-protein interaction affinity upon screening of the protein surface charges. These findings and the proposed methodology are of high interest particularly for structural biology and applications reliant on protein crystallization, including the development of novel biomaterials.

1. Introduction

Interactions between macromolecules are key to understanding their phase behavior. Effective interactions between proteins in solution are defined by the interplay between electrostatic repulsion, van der Waals attraction, and less clearly defined hydration and hydrophobic contributions [1]. These interactions define macromolecular solubility and organization at the cellular level and are of great importance for numerous pathological problems linked to protein aggregation [2,3].

In vitro, controlling these interactions is essential for high-quality crystal production required for structural biology studies, and also for pharmaceutical formulation [4], or bio catalysis [5], among other different research fields and applications. In this regard, proteins have historically been central to crystal nucleation studies, including the development of the Two-Step Nucleation theory [6]. Moreover, recent advancements in material science highlight the use of protein crystals as porous materials for drug delivery and catalysis [7]. However, optimizing crystallization conditions to achieve the desired crystal size and quantity often relies on trial-and-error approaches, which highlights the importance of systematically understanding protein interactions and their characterization.

Small Angle X-Ray Scattering (SAXS) has proven itself as a powerful tool for studying macromolecular interactions [1,8–11]. However, the relatively limited access to synchrotron beamlines, and the complexity of data analysis remain common obstacles to applying SAXS in routine screening. Here, we propose Fluorescence Lifetime Imaging Microscopy (FLIM) with molecular rotors as a more accessible technique for probing protein interactions.

Molecular rotors are fluorophores with the property of intramolecular rotation [12]. Their fluorescence lifetime is influenced by the surrounding environment: hindered rotation due to viscosity or molecular interactions leads to longer lifetimes, while free rotation in less restrictive environments yields shorter lifetimes (for more details, see the molecular rotors section in the supporting information) [13]. Fluorescence Lifetime Imaging Microscopy (FLIM) provides spatially-resolved imaging of fluorescence lifetimes, offering insights into the sample's local environment [14].

FLIM has been widely applied in biological research, where

* Corresponding author.
E-mail address: isaac.rodriguez-ruiz@cnrs.fr (I. Rodriguez-Ruiz).

https://doi.org/10.1016/j.molliq.2024.126350
Received 28 June 2024; Received in revised form 15 October 2024; Accepted 24 October 2024
Available online 28 October 2024

molecular rotors have been used for measuring micro-scale viscosity in cellular compartments and membranes [15–18]. Molecular rotors have provided important insights into the structural changes within cells due to protein aggregation associated with neurodegenerative diseases [13,19,20]. For example, $DiSC_2$ rotor revealed the different stages in lysozyme's transition to amyloid fibrils gel [13], while BODIPY rotors highlighted the viscosity differences between the dense liquid phases of Tau self-coacervation and RNA-Tau coacervation complexes [21].

While these studies have provided valuable insights into protein environments during phase transitions, they have not specifically targeted parameters relevant to protein crystallization. Prior research using molecular rotors and other fluorescent probes has effectively detected specific biomolecular interactions upon the target binding of the fluorophore to the interacting molecules [22–24]. However, the application of non-conjugated free molecular rotors for characterizing non-specific protein–protein interactions in the context of protein phase transition has not yet been explored. This study aims to advance this approach and examines how the fluorescence lifetime of non-conjugated molecular rotors relates to non-specific protein interactions in solution, thereby providing insights into solubility data relevant to protein crystallization.

2. Experimental section

2.1. Solutions preparation

During the FLIM experiments, protein-salt mixtures were prepared directly in ELISA well-plates under mineral oil to avoid the solution evaporation. Each sample droplet had a total volume of 15 μL and consisted of a mixture of protein, buffer, salt and molecular rotor stock solutions (see supporting information for further details on solution preparation). Given the time frame of the measurements (a few minutes maximum between the reagents mixing and the fluorescence lifetime measurement), water diffusion into the mineral oil can be considered negligible. For the protein solutions prepared under supersaturated conditions (i.e. in non-equilibrium conditions overcoming protein solubility), and to avoid their crystallization/precipitation during the experiments, measurements of the fluorescence lifetime were conducted immediately after the mixing of the components, while supersaturated solutions remained in a metastable state for hours.

The water-soluble molecular rotor, Sulforhodamine-B (SRB), was chosen for this study due to its well-documented high affinity for proteins [25], making it a promising candidate for investigating protein interactions. Its water solubility eliminates the need for solvents like DMSO, which are commonly required for non-water-soluble probes and could potentially alter the protein system state. SRB has an excitation/emission maximum at $\lambda_{Ex}/\lambda_{Em} = 565/586$ nm. For the preparation of the samples, SRB was added to the final concentration of 0.1 mM into the analyzed mixtures. The choice of this concentration stems from the fact that the rotor was excited at sub-optimal conditions ($\lambda = 515$ nm, far from its maximum absorption at 565 nm), thus also obtaining sub-optimal emission yield. To experimentally optimize the signal-to-noise ratio, while avoiding collisional quenching effects, that could decrease the rotor lifetime, and the self-absorption of photons giving rise to artificial longer lifetimes, preliminary measurements of SRB fluorescence lifetime were conducted in aqueous solutions across various SRB concentrations. In the current experimental setup and operational conditions, fluorescence lifetime measurements in water were revealed to be independent on the dye concentration at dye concentrations up to 0.3 mM. Additionally, all the fluorescence lifetime measurements were performed at constant temperature to account for the rotor's temperature sensitivity [26].

2.2. Fluorescence Lifetime Imaging Microscopy (FLIM) measurements and data analysis

Fluorescence lifetime measurements were performed using a frequency domain FLIM camera system (PCO.FLIM, Excelitas technologies, USA) [27] mounted on Leica DMi8 Inverted Microscope (Leica Microsystems, Germany). The measurements were performed utilizing a laser (model pco.Laser 515.110 LLG, OMICRON, Germany) with an excitation wavelength of 515 nm. The laser was modulated at 40 MHz frequency (being the maximum attainable by the experimental setup). Laser excitation signal was filtered with a high-pass filter 500–520 nm. To recover the fluorophore emission, an emission filter with a window of 570–640 nm was used.

The emission signal experiences a phase shift and a decrease in amplitude (demodulation) due to the finite value of the fluorescence lifetime. From this phase shift and amplitude change, fluorescence phase and modulation lifetimes were automatically calculated using NIS Elements software. In the cases in which one fluorophore reports on a homogeneous environment with a corresponding single value of the lifetime (monoexponential fluorescence decay), phase and modulation lifetimes are equal. Otherwise, fluorescence decay is multiexponential, indicating that during the measurement, more than one fluorophore is present in the system, or that a single fluorophore is present in different states. In this work, all the results were presented in terms of the fluorescence phase lifetime, as it is less sensitive to the room light pollution [28] and to the modulation frequency limitations [29].

To calculate the average fluorescence lifetime for each measurement, the fluorescence lifetimes distribution data corresponding to a 1008 × 1008 pixels images were exported and processed using an ad-hoc Python code. Experiments were triplicated for each tested condition, and within each sample, the fluorescence lifetime was measured three times. The final lifetime value was obtained by averaging the results of these 3 × 3 measurements. The error bars for each experimental condition were computed as the sum of three components: the deviation from the lifetime distribution of each individual measurement, the deviation among three measurements within each sample, and deviation among three independent samples for each tested condition. The confidence level for these calculations was set at 95 %.

Complementary measurements were performed in time-domain single photon counting FLIM, allowing for the direct reconstruction of the fluorescence decay. The time-resolved fluorescence lifetime experiments were conducted using an Abberior Expert Line confocal microscope (Abberior Instruments GmbH, Germany). The excitation source was a 560-nm pulsed diode laser, working at a repetition rate of 40 MHz. Fluorescence detection was performed on a silicon avalanche photodiode detector (SPAD, Perkin Elmer SPCM-AQRH-14) after a 580–630 nm bandpass filter. Single photon time-tagging was performed using HydraHarp 400 electronics (PicoQuant GmbH, Germany). Given the optimal excitation conditions and the very high sensitivity of the point SPAD detector in confocal mode, the final SRB concentration in protein solutions was readjusted to 0.1 nM. Otherwise, the preparation of the protein solutions was analogous to that previously described. Raw FLIM images of 10 × 10 μm^2 with a pixel size of 40 nm were obtained with an acquisition time of 1 ms per pixel. The analysis of fluorescence decay traces in individual pixels was performed using SymphoTime 64 (PicoQuant) software. For an accurate pixelwise analysis and achieving higher photon counts per pixel, a pre-treatment consisting on a spatial binning of 10 × 10 pixels and a temporal binning of 16 channels was performed for each FLIM image. To account for potential different environments and photophysical processes of the dye, the FLIM images were fitted, pixelwise, to a two-exponential decay function. The resulting frequency distributions of the lifetime components were exported and fitted with a Gaussian distribution function using a custom Python code. In each tested solution, measurements were triplicated.

2.3. Small angle X-ray scattering (SAXS)

Small-angle X-ray scattering (SAXS) experiments were conducted on a XEUSS 2.0 laboratory setup (Xenocs) equipped with a Pilatus 1 M HPC detector (DECTRIS) and a Cu X-ray source ($\lambda = 1.54$ Å) from GeniX3D.

The experiments were performed at the fixed sample-to-detector distance of 1216 mm to obtain signals in the q range of 0.009–0.5 $Å^{-1}$ with an X-ray flow close to 120 M ph/s. The samples were injected through a low noise scattering cell coupled to a homemade automated sample injector. Three acquisitions of 600 s were averaged for each sample with buffer subtraction. SaSView 5.0.4 software was employed to analyze the SAXS signals of lysozyme solutions.

SAXS analyses were performed on lysozyme solutions of 70 mg/ml with NaCl concentrations varying from 0 to 3 % w/v. The protein–-protein effective interactions were analyzed by comparing the structure factors of the solutions with increasing salinity, in the absence and in the presence of SRB rotor at a 0.1 mM concentration. The form factor of lysozyme, representing the scattering signal in the absence of protein interactions in the solution was measured on a diluted lysozyme solution of 3 mg/ml.

2.4. X-ray diffraction (XRD)

Lysozyme crystals were obtained using the hanging drop vapor diffusion method set-up in 24 well plates (HR, USA) and kept at 293 K for equilibration. Lysozyme stock solution prepared in 50 mM NaOAc pH 4.5, was mixed with buffered SRB to reach a final concentration of 25 mg/ml of protein and 0.1 or 0.3 mM of SRB, respectively. Drops were prepared by mixing 1 μl of protein solution with 1 μl of precipitant (1.5 M NaCl in 50 mM NaOAc pH 4.5) in a siliconized glass cover slip and flipped over the well containing 500 μl of the precipitant solution.

Lysozyme crystals stained with SRB exhibited a characteristic pink color so that they were easily identified under a microscope (see Fig. S3 in the supporting information), fished with the help of a litto loop and transferred to a 5 μl drop of mother solution containing 15 % (v/v) glycerol as cryo-protectant. After soaking for less than 30 s, crystals were flash-cooled in liquid nitrogen before data collection. X-ray diffraction data were collected at XALOC beamline (ALBA, Barcelona, Spain). Diffraction frames were processed with autoPROC [30], and merged, scaled and reduced using Aimless from the CCP4 suite [31,32]. The crystal structure of lysozyme was determined by the molecular replacement method using the high-resolution 3D model (PDB ID. 1IEE) as the search model in Molrep [33]. Refinement was carried out with REFMAC [34] from the CCP4 suite. Water picking, manual refinement, and electron density maps inspection was done with COOT [35].

3. Results

3.1. SRB fluorescence lifetime measurements in lysozyme solutions

To assess the sensitivity of SRB to viscosity, a series of water/glycerol mixtures were prepared, with glycerol content ranging from 0 to 50 % v/v, resulting in viscosities ranging from 0.93 to 7.4 cP. The fluorescence lifetime (τ) value of 2.13 ns for a 30 % glycerol solution was chosen as the reference for phase-modulation lifetime measurements [36]. The fluorescence lifetime trend for SRB showed the expected behaviour in response to varying viscosity, consistent with previously reported data [37] (Fig. 1, red dots series).

Subsequently, the correlation of SRB fluorescence lifetime values with macroscopic viscosity of lysozyme protein solutions (10–210 mg/ml) was investigated. The corresponding viscosities of the solutions were calculated from the experimental fit obtained by Fredericks *et al.* [38]. The observed evolution of the SRB fluorescence lifetime did not align with the calibration curve established for water-glycerol mixtures. Within the concentration range of 10–80 mg/ml, τ exhibited a high sensitivity to lysozyme concentration, increasing faster with respect to the macroscopic viscosity-driven expectations. As the concentration exceeded 80 mg/mL, the fluorescence lifetime plateaued, remaining below the τ values associated with the macroscopic viscosity. This suggests that the evolution of SRB fluorescence lifetime with increasing lysozyme concentration cannot be merely attributed to variations in the

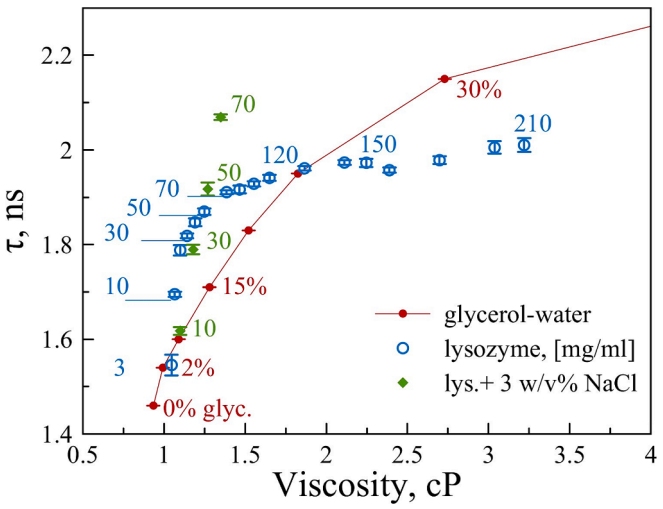

Fig. 1. SRB fluorescence lifetime (τ) as a function of viscosity in water/glycerol mixtures of increasing glycerol content (in %v/v of glycerol); in lysozyme solutions of increasing concentration (numbers specify corresponding concentration of lysozyme in mg/ml); and in lysozyme solutions of increasing concentrations (10, 30, 50, 70 mg/ml) upon addition of 3 % w/v NaCl. Error bars for τ measurements in glycerol solutions were calculated from the fluorescence lifetimes distribution data of a single measurement per condition.

macroscopic solution viscosity. The obtained trend agrees with the reported behaviour for a similar molecular rotor, rhodamine, in whey protein solutions, where the lifetime trend is attributed to non-specific interactions between the probe and the protein [39].

The presence of protein-SBR interactions was supported by a higher degree of multi-exponentiality with respect to the measurements in water-glycerol mixtures (see supporting information: phasor plot analysis). This suggests that the rotor reports on several environments, plausibly due to the presence of interactions between SRB and lysozyme and multiple sites on the surface of protein with which rotor can interact, changing the energy barrier for intramolecular rotation of SRB [19].

The addition of salt is known to modify protein–protein interactions by screening surface charges and potentially promoting attraction between protein molecules, thereby affecting average intermolecular distances. Therefore, to further investigate the nature of lifetime changes in lysozyme solutions, NaCl was added to the protein solution. The fluorescence lifetime values of SRB in protein solutions with lysozyme concentrations of 10, 30, 50, 70 mg/ml, containing 3 % w/v NaCl are depicted in Fig. 1 (green diamonds series). According to Fridericks *et al.*, the viscosity of lysozyme solutions does not significantly vary with the addition of salt [38]. However, the fluorescence lifetime measurements appeared to be highly influenced by the introduction of NaCl, displaying a decrease of τ in 10 and 30 mg/ml solutions followed by a pronounced increase of τ, notably surpassing the concentration-driven changes in 50 and 70 mg/ml solutions in the absence of salt.

3.2. Lifetime measurements and protein interactions

To systematically analyse the observed trends, the effect of increasing NaCl concentration (from 0 to 7 % w/v) was studied in lysozyme solutions of four different concentrations (10, 30, 50, 70 mg/ml). The phase diagram of lysozyme in the presence of NaCl as precipitant (pH 4.5, T = 22.7 °C) has been previously reported [40], making it possible to interrogate the system with respect to protein solubility conditions as a function of protein and salt concentration. To compare different conditions in terms of protein and salt concentrations, the obtained fluorescence lifetime values were plotted as a function of the supersaturation *S* (Fig. 2, A), defined as:

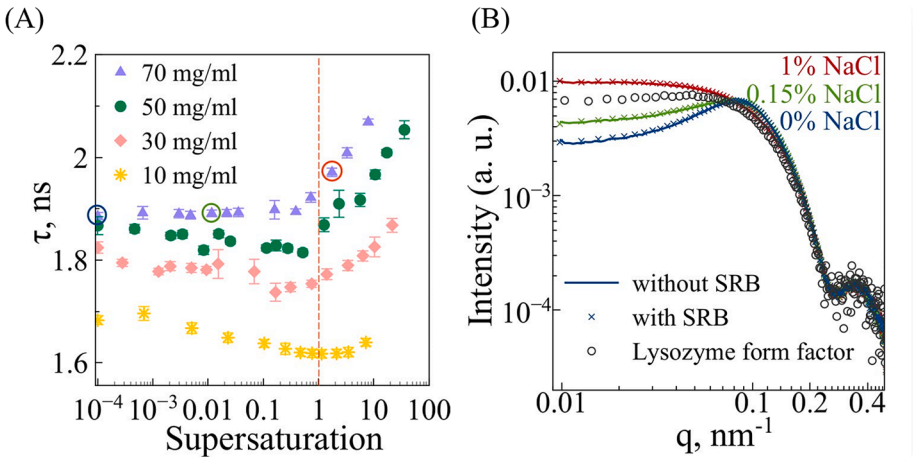

Fig. 2. (A) SRB fluorescence lifetime as a function of supersaturation in different lysozyme solutions at concentrations of 10, 30, 50, 70 mg/ml. (B) SAXS curves for 70 mg/ml lysozyme solutions at the salt concentration conditions corresponding by colours to the ones chosen on the lifetime plot (blue, 0 % NaCl, green, 0.15 % NaCl, red, 1 % NaCl).

$$S = \frac{C_{prot}}{solubility(T, C_{salt})} \quad (1)$$

where c_{prot} is a given concentration of protein and $solubility(T,\ c_{salt})$ is the equilibrium protein solubility concentration at given conditions of temperature T and salt concentration c_{salt}. It is worth noting that supersaturation is the main driving force for phase transition, and that it plays a major role in dictating the physico-chemical properties of the solid material, such as structure, morphology and particle size.

Remarkably, all the curves exhibited a similar non-monotonous trend as a function of supersaturation, with τ remaining nearly constant and slightly decreasing under highly undersaturated conditions, followed by a subsequent growth starting close to the protein solubility ($S = 1$) and persisting with the increase of supersaturation level in the solutions (all the fluorescence lifetime measurements were conducted before any precipitation occurs, i.e. in the bulk homogeneous metastable solutions).

To elucidate the correlation between the fluorescence lifetime and the protein solution dynamics, SAXS analyses were additionally conducted on the protein solutions examined with FLIM (Fig. 2, B). By comparing these curves to the form factor of lysozyme, which represents the absence of interactions between the protein molecules, a peak in the higher q range, indicative of repulsive protein interactions, was observed in the cases of 0 % w/v and 0.15 % w/v NaCl. Conversely, in the lysozyme solution containing 1 % w/v NaCl, the previous peak was not present, whereas an increasing slope in the lower q range was observed, pointing out to attractive interactions. Hence, the observed change in the fluorescence lifetime can be related to the transition from a repulsive to an attractive interaction state between the protein molecules.

It is worth noting that significant differences between the SAXS curves in the presence and the absence of SRB were not observed, indicating that the rotor does not alter the system's dynamics and merely acts as a probe for measuring protein interactions. Additionally, preferential protein-SRB binding interactions were examined by X-ray diffraction. Firstly, lysozyme crystals were soaked in an SRB solution. The initially transparent crystals became stained in pink after a few minutes, while the solution was gradually depleted in SRB, demonstrating preferential interactions between SRB and the protein. However, X-ray diffraction crystallographic analyses did not show any extra electron density around the protein molecules, which could be attributed to SRB. Subsequently, lysozyme was directly crystallized in the presence of SRB at two different concentrations of 0.1 and 0.3 mM. Several crystals nucleated and grown in the SRB environment were measured at X-ray diffraction synchrotron facilities. All crystals diffracted at a resolution better than 1.7 Å, even down to 1.0 Å for one of them. After performing analyses for molecular replacement and water positioning, none of the diffracted crystals presented any extra density compatible with the SRB moiety, therefore indicating a non-specific interaction between SRB and lysozyme.

3.3. *Effect of precipitant and macromolecule nature on SRB fluorescence lifetime*

To examine a broader applicability of the rotor as a probe for protein interactions, the influence of the nature of different precipitant agents, macromolecule species and pH was studied.

Additional FLIM analyses were conducted using a stronger precipitant from the Hoffmeister series, sodium nitrate [41]. Analogous to the case of NaCl, the solubility of lysozyme in $NaNO_3$ solutions at pH 4.5 is known from the literature [42], making it possible to directly compare the SRB fluorescence lifetime with the previous experiments in the presence of NaCl, as a function of supersaturation. The obtained trends in the fluorescence lifetime of SRB in protein solutions containing $NaNO_3$ were similar to those containing NaCl, displaying an equivalent change in the fluorescence lifetime trend in the vicinity of protein solubility (Fig. 3, A). In contrast, under undersaturated conditions, the slight decrease of τ was not clearly observed, as it was when using NaCl.

Subsequently, a series of measurements were conducted using sodium sulphate as a precipitant. In this case, the solubility data of lysozyme as a function of sodium sulphate concentration at pH 4.5 has not been previously reported to the best of our knowledge. Hence, and for the sake of comparison, the results are presented as a function of unknown supersaturation values, scaled to the results obtained with NaCl (Fig. 3, B). A change in the fluorescence lifetime trend was detected around the condition in which the first lysozyme precipitate appeared within the next 24 h after the FLIM measurement (see Fig. S4 in the supporting information). This finding suggests that with a simple screening of conditions and by using the molecular rotor as a probe, it is possible to qualitatively predict the solubility of the protein when specific solubility data are not available, as well as getting an estimate of supersaturation conditions. This can potentially and greatly facilitate the screening for protein crystallization conditions in structural biology and biomaterials related studies.

Further, the same experimental approach was implemented to study how the fluorescence lifetimes of SRB in protein solutions are affected by the presence of non-ionic precipitant agents as polyethylene glycol (PEG). PEG is known to induce depletion interactions between proteins, decreasing their solubility. To estimate the effect of the viscosity of PEG-

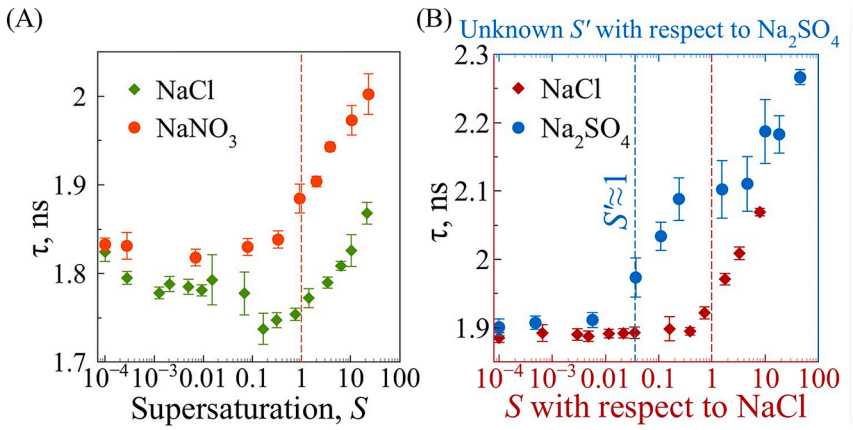

Fig. 3. SRB fluorescence lifetime as a function of supersaturation in 30 mg/ml and 70 mg/ml lysozyme solutions upon the addition of $NaNO_3$ (A) and Na_2SO_4 (B), respectively, compared to the case with NaCl. The data for Na_2SO_4 was scaled to the NaCl solubility for the convenience of representation, while the real solubility is around the condition marked by blue dashed line ($S' = 1$), where the first precipitate was observed.

3350 on the fluorescence lifetime, a series of experiments were performed in different PEG – water and PEG – 50 mg/ml lysozyme mixtures, increasing the polymer concentration. It can be observed that at concentrations higher than 5 % v/v of PEG, τ measurements are highly dominated by the viscous contribution of PEG, as the τ in protein-containing solutions closely follows the values in PEG solutions without the protein (Fig. 4, A).

Subsequently, τ measurements were performed in the presence of 5 % v/v and 25 % v/v of PEG-3350 (Fig. 4, B) for a series of increasing NaCl concentrations on a fixed 30 mg/ml lysozyme solution. The data for the PEG-containing solutions wer scaled to the NaCl solubility for the convenience of representation, while the real solubility was found to be around the conditions marked by dashed lines ($S'_{25\%}$ and $S'_{5\%}$ for the mixtures containing 25 % and 5 % v/v PEG-3350, respectively), where first crystals were observed. When comparing the results with the trend obtained in the absence of PEG, it can be noticed that at 5 % v/v PEG, where the viscous contribution of PEG still does not dominate the τ values over the SRB-protein τ contribution, the observed trend is similar, but the increase of τ above solubility is less pronounced.

However, at 25 % v/v PEG, the observed trend was reversed. At low salinities, τ remained nearly constant and fluctuated around 2.18 ns, which corresponded to the fluorescence lifetime in 25 % v/v PEG solution without the protein. Notably, the fluorescence lifetime measurements exhibited a much lower degree of multiexponentiality than those from protein solutions without PEG. This indicates that the interactions between the probe and the polymer (resulting in a single exponential decay) dominate over the interactions between the probe and the proteins, and the viscosity of the polymer solution defines the fluorescence lifetime. At conditions close to the solubility, τ started to decrease below the value corresponding to the 25 v/v% PEG solution, indicating a change in the rotor's environment. These findings show that in the presence of PEG in the solution, the fluorescence lifetime of SRB is strongly affected by the contribution of the polymer to viscosity. In this case, and considering the weight of these interactions on the global trend of the lifetime, even though the information related to protein interactions is still valuable, its interpretation can be more ambiguous.

Finally, the same methodology was applied to another protein, BSA, under two distinct conditions: at pH 3.7, at which BSA has a positive net charge, and at pH 7 (MilliQ Water), at which BSA has a negative net charge (the isoelectric point of BSA is around 4.7). Previous measurements conducted in buffer solution in the absence of protein with varying pH levels (3.7, 4.5, and 7) have shown that the fluorescence lifetime of SRB remains largely unaffected by changes in pH (see Fig. S6 in the supporting information). We conducted SRB lifetime measurements over a broad range of salt concentrations (0–11 % w/v NaCl) in 40 mg/ml BSA solutions. As the solubility data for BSA in the screened conditions were not known, the resulting τ trends were plotted as a function of NaCl concentration on a logarithmic scale to make them

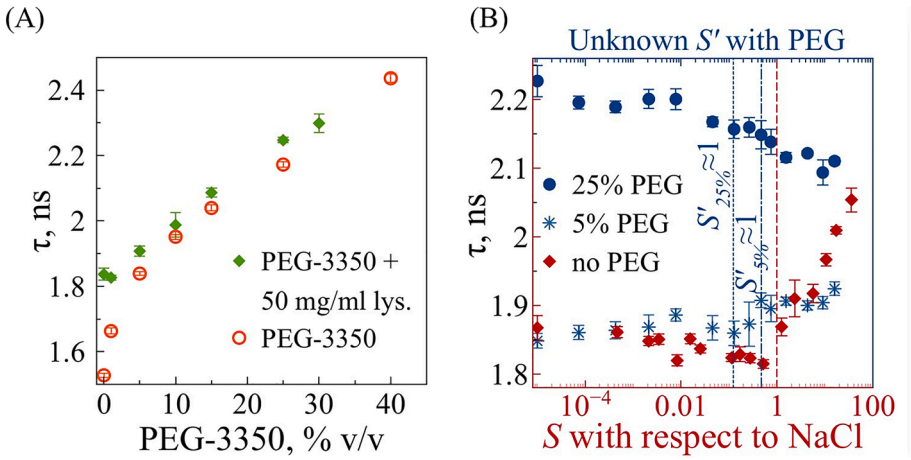

Fig. 4. (A) Comparison of the fluorescence lifetime in the PEG-3350/water and PEG-3350/50 mg/ml lysozyme mixtures with increasing PEG content. (B) Comparison of the fluorescence lifetime as a function of supersaturation in the 30 mg/ml lysozyme solutions upon the addition of NaCl in the presence of 0, 5 and 25 % of PEG-3350.

comparable with the previous experiments with lysozyme, represented in supersaturation terms (Fig. 5, A).

At pH 3.7, a trend similar to that obtained for lysozyme solutions was observed, with a slight decrease of τ at low salt concentrations, followed by a pronounced growth at high salinities. In the increasing τ region (NaCl concentration range from 3 to 11 % w/v), the solutions precipitated within 48 h after the measurements, confirming attractive interactions and supersaturation under these conditions (see Fig. S5 in the supporting information). In plane water, amyloid formation was observed in the two last conditions (10 and 11 % w/v NaCl) within 48 h. Further, the lifetime analysis was compared to the SAXS results reported in the literature for the same conditions.

Zhang *et al.* studied the interactions in BSA solutions in pure water (expected pH ~ 7.0) over a range of ionic strengths from 0 to 2 M, corresponding to 0 to 11.7 % w/v NaCl [8]. SAXS analyses of the solutions revealed that in the region from 0 to 1.2 % w/v NaCl (0–0.2 M), the effective protein interactions were repulsive and could be modelled by a screened Coulombic potential. In the presented lifetime analysis, this corresponds to the region with decreasing lifetime as NaCl concentration increased (Fig. 5, B). From 1.2 to 4.1 % w/v NaCl (0.2–0.7 M), the surface charge of BSA was screened and SAXS curves were fitted using the BSA form factor, implying the absence of effective interactions. Accordingly, the fluorescence lifetime of SBR experienced a change towards and inflection point in this region, and globally, it remained nearly constant. Finally, at high ionic strength (where τ increased with NaCl concentration), the interactions were found to be attractive and SAXS data were fitted to an attractive square-well potential. Thus, the FLIM analysis presented herein is in perfect agreement with Zhang *et al.*'s SAXS findings, and captures effectively the transitions between the distinct interaction regimes in BSA solutions.

4. Discussion

The sensitivity of the fluorescence lifetime of SRB to the transition from the repulsive to the attractive interaction regime in protein solutions can be related to the interactions between the rotor and the protein. These interactions are characterized by a complex interplay of various forces, including van der Waals attractions, electrostatic repulsion/attraction, hydrophobic π-π interactions involving the aromatic groups of the probe and the protein surface, as well as hydrogen bonding [43]. Previous research on this subject has extensively examined the interactions between globular proteins like lysozyme, BSA, and Human Serum Albumin (HSA) with various fluorophores using spectroscopic techniques and molecular docking [44–50]. These studies suggest that the nature of the forces dominating the probe-protein interactions is highly dependent on the protein surface and the probe chemical structure. Introducing salt into the protein solution causes counter-ions to bind to the charged moieties on the protein's surface, leading to alterations in both protein–protein interactions and the protein's conformation and microenvironment [51]. These changes subsequently can influence the interactions between the probe and the protein.

Representing the data for lysozyme and BSA solutions in the presence of different NaCl concentrations (corresponding to the Fig. 2 and Fig. 5, respectively) on the phasor plot – a graphical method used in FLIM to analyze multiexponential decay (see supporting information for more details on phasor plot analysis)-provides key insights into the mechanisms behind the observed lifetime changes (Fig. 6, A). The lifetime points fall within the universal semicircle, indicating the multiexponential nature of the decay. All the data points align on an imaginary line connecting two distinct lifetime values of two rotor populations: one population corresponds to the free rotor in water, while the other presumably represents the rotor interacting with the protein. The distance of each data point from these values is proportional to the relative quantity of the rotor population in the solution, following the lever rule.

Complementary FLIM measurements using a single-photon counting microscope confirmed the multiexponential decay kinetics observed with frequency-domain FLIM. FLIM images were fitted pixelwise to a two exponential decay function, accounting for different environments of the fluorophore. The intensity-averaged lifetime ($\tau_{av\ int}$, Eq. (2)) repeated the trend obtained from the frequency-domain measurements (see Fig. S7 in the supporting information).

$$\tau_{avint} = (\tau_{short}^2 A_{short} + \tau_{long}^2 A_{long})/(\tau_{short} A_{short} + \tau_{long} A_{long}) \quad (2)$$

Here τ_{short} and τ_{long} are the two lifetime components with the respective population weights of A_{short} and A_{long}. The product $\tau_i A_i$ represents the fluorescence intensity of the respective fluorophore population.

The obtained fluorescence lifetime histograms from FLIM images (Fig. 6, B) have shown that the weight ratio between the two states in which SRB is presented in the solutions changes upon the addition of NaCl, in agreement with the phasor plot analysis. The short lifetime component (1.7 *ns*), corresponding to the τ in water in the absence of protein, dominates the average fluorescence lifetime in undersaturated protein solutions. In the protein-free buffer solutions (see supporting information Fig. S8), the addition of NaCl led to a slight decrease in fluorescence lifetime, likely caused by dynamic quenching due to Cl^- ions. This suggests that the minor reduction in average fluorescence lifetime observed in the repulsive interaction regime can be attributed to Cl^- quenching. In contrast, $NaNO_3$ did not cause a similar initial lifetime

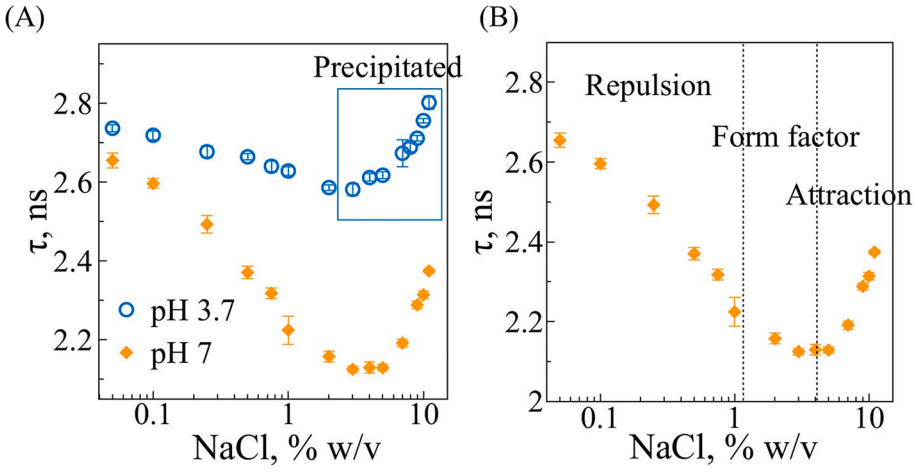

Fig. 5. (A) Fluorescence lifetime evolution in 40 mg/ml BSA solutions at pH 3.7 and at pH 7 as a function of NaCl concentration. (B) Superimposition of SAXS-fitted interaction regimes with the FLIM data for 40 mg/ml BSA solution at pH ~ 7.

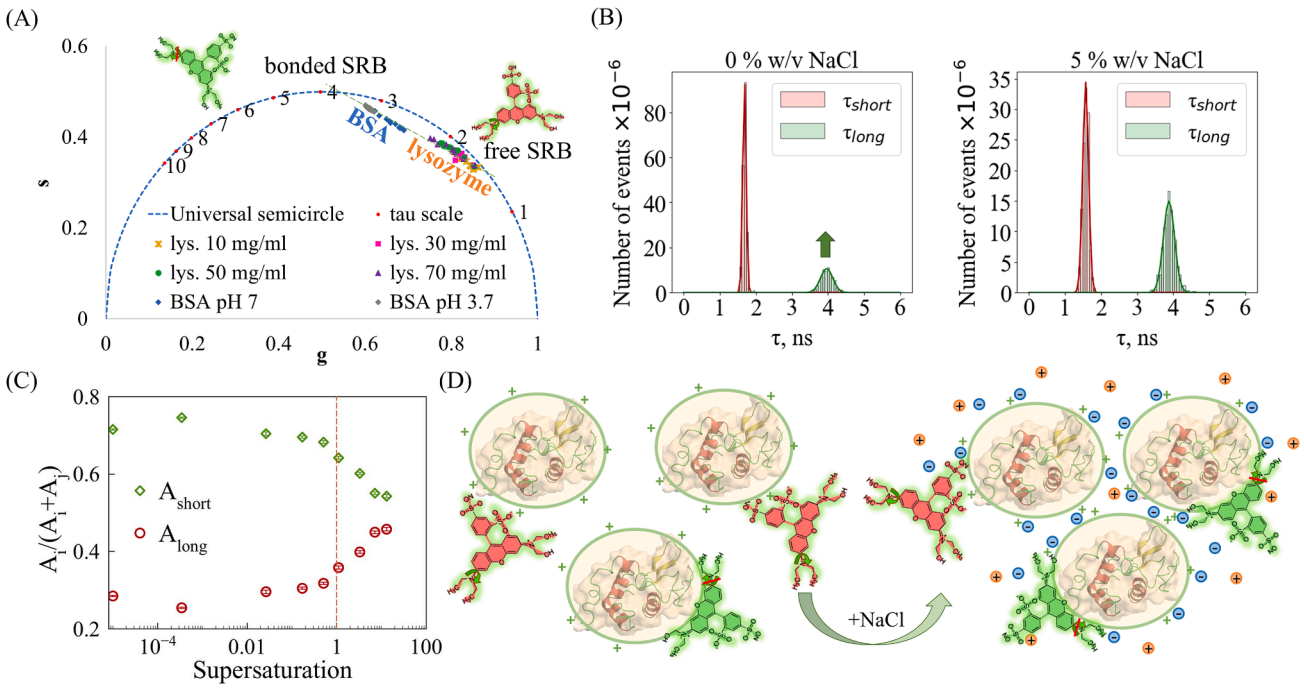

Fig. 6. (A) Phasor plot for the fluorescence lifetime in lysozyme and BSA solutions upon the addition of NaCl. (B) Lifetime histograms with Gaussian fits collected from FLIM images of 50 mg/ml lysozyme solution with 0 % w/v NaCl and 5 % w/v NaCl. (C) Relative weights of fluorophore populations in protein solutions as a function of supersaturation in the solutions. Presented error bars correspond to three measurements in a single solution. (D) Illustration of the proposed mechanism underlying SRB sensitivity to protein interactions.

reduction, further confirming that Cl^- ions are responsible for the quenching effects.

The long lifetime component (3.9 *ns*) is expected to be attributed to the population of the fluorophore interacting with the protein. Studying the trends of the relative fluorophore population weights ($A_{short} + A_{long} = 1$) with the salt addition reveals that the screening of the protein surface charge, close to the protein solubility ($S = 1$), enhances the interaction between the protein and SRB (Fig. 6, C). Thus, the average τ increase in the attractive interaction regime can be explained by an increase in the weight of the long-lifetime SRB population. High lifetimes in BSA solutions (Fig. 5) due to the larger quantity of bonded SRB in BSA solutions (Fig. 6, A) could be explained by the much larger size of BSA in respect to lysozyme, allowing for a higher binding capacity of SRB, even at low salt concentrations.

It is conceivable that both populations of SRB are located on the protein surface, with the difference in the lifetime (τ_{short} and τ_{long}) dictated by the orientation of the probe on the surface: for the short-lifetime component, the rotating groups of SRB are oriented towards the solution and their rotation is dictated by the immediate environment of the protein, while for the long-lifetime component, upon the screening of the protein surface charge, the rotor is in the position restricting the mobility of the rotating groups, leading to higher values of the fluorescence lifetime (Fig. 6, D). For 25 % v/v PEG solutions, the decrease in lifetime in supersaturated solutions could be attributed to the exclusion of PEG from the inter-protein space. As proteins approach each other and their excluded volumes overlap in the attractive interaction regime, the probe with the rotating groups oriented towards the solution may find itself in a less viscous environment compared to the 25 % v/v PEG solution, resulting in the decrease of τ.

Importantly, the results indicate that in protein solutions containing added salt, the inherent viscosity of the protein solution does not affect the fluorescence lifetime, and only the variations in the protein-probe interactions define the fluorescence lifetime change. Additionally, for future applications of SRB in screening crystallization conditions, it is essential to conduct analyses at a constant temperature (as was done at room temperature in this study). SRB's fluorescence lifetime is highly sensitive to temperature [26], making it necessary to maintain constant temperature conditions to ensure that the observed lifetime changes are attributed to protein interactions rather than temperature variations.

5. Conclusions

In this study, the potential of Fluorescence Lifetime Imaging Microscopy (FLIM) to examine intermolecular protein–protein interactions was investigated by utilizing the commercial molecular rotor SRB as a probe in protein solutions. Results indicate that the fluorescence lifetime of SRB is a powerful indicator for tracking the transition between repulsive and attractive interaction regimes within protein solutions, displaying a notable increase in the fluorescence lifetime around the solubility threshold. Consistent experimental observations for lysozyme in the presence of different salts (NaCl, $NaNO_3$, Na_2SO_4) and PEG-3350 as precipitants, and for BSA at pH above and below its isoelectric point using NaCl as precipitant, suggest that SRB can be employed for studying protein interactions across a wide spectrum of conditions. Based on the experimental evidence, a hypothesis regarding the mechanism underlying the sensitivity of SRB fluorescence lifetime to protein interactions is presented. The interplay of simultaneous protein–protein and protein-probe attractive interactions contribute to the observed fluorescence lifetime increase, while the viscosity of the protein did not show a direct effect on the lifetime changes.

The approach proposed in this paper expands the toolkit for structural biology and protein/biomolecule crystallization research by facilitating and rationalizing phase transitions and thus screening crystallization conditions. This method is particularly valuable for applications requiring fine control of the structure and final crystal size dictated by the supersaturation level, such as the development of novel biomaterials. Moreover, the experiments proposed with different precipitant agents highlight the utility of this methodology for studying the Hoffmeister series in protein solutions. This method may be of general application using other suitable molecular rotors for studying protein

interactions and phase transitions. However, prior to applying a specific rotor to a particular protein of interest, the presence of probe-protein interactions should be corroborated.

CRediT authorship contribution statement

Yevgeniya Karibjanova: Writing – original draft, Visualization, Methodology, Investigation, Formal analysis, Conceptualization. **Isaac Rodriguez-Ruiz:** Writing – review & editing, Writing – original draft, Supervision, Project administration, Methodology, Investigation, Funding acquisition, Conceptualization. **Angel Orte:** Writing – review & editing, Supervision, Investigation, Formal analysis. **José Antonio Gavira:** Writing – review & editing, Investigation, Formal analysis, Conceptualization. **Pierre Roblin:** Investigation, Formal analysis. **Sébastien Teychené:** Writing – review & editing, Supervision, Project administration, Methodology, Investigation, Funding acquisition, Formal analysis, Conceptualization.

Declaration of competing interest

The authors declare that they have no known competing financial interests or personal relationships that could have appeared to influence the work reported in this paper.

Acknowledgements

This work was supported by the projects ANR 2021 TITANS, France, and LP-to-CRYST ETI 2024 of Toulouse INP University, France.

YK has received financial support through a PhD grant from French Ministry of higher education, France.

Data collection were performed at the XALOC beamline of the Spanish Synchrotron radiation source, ALBA (Barcelona), Spain with the help of the ALBA staff. JAG is supported by the Spanish Ministry of Science and Innovation/FEDER funds Grant PID2020-116261GB-I00, AEI/10.13039/501100011033, Spain.

YK expresses gratitude to Prof. Marina K. Kuimova from the Imperial College London for her valuable insights and discussions during the initial phase of this work.

YK gratefully acknowledges Research Engineer E. Cid from the Laboratory of Chemical Engineering of Toulouse for his valuable assistance with the experimental FLIM setup.

Appendix A. Supplementary data

Supplementary data to this article can be found online at https://doi.org/10.1016/j.molliq.2024.126350.

Data availability

The Supporting Information includes the experimental details on the solutions preparation, detailed introduction to molecular rotors and phasor plot analysis, and supporting figures listed below. S1. Energy landscape of a molecular rotor undergoing TICT. S2. Schematic representation of a phasor plot. S3. Pink SRB-stained lysozyme crystals for X-Ray Diffraction analysis. S4. Precipitation in lysozyme solutions upon addition of Na_2SO_4. S5. Precipitation in BSA solutions at pH 3.7 upon addition of NaCl. S6. Fluorescence lifetime evolution with pH. S7. Fluorescence lifetime evolution comparison for Frequency Domain FLIM and single photon counting FLIM. S8. Fluorescence lifetime evolution with NaCl concentration. S9. Time-domain fluorescence decay traces at varying NaCl concentration.

References

[1] A. Tardieu, A. Le Verge, M. Malfois, F. Bonneté, S. Finet, M. Riès-Kautt, L. Belloni, Proteins in solution: from X-ray scattering intensities to interaction potentials, J. Cryst. Growth 196 (1999) 193–203, https://doi.org/10.1016/S0022-0248(98)00828-8.

[2] Y.S. Eisele, C. Monteiro, C. Fearns, S.E. Encalada, R.L. Wiseman, E.T. Powers, J. W. Kelly, Targeting protein aggregation for the treatment of degenerative diseases, Nat. Rev. Drug Discov. 14 (2015) 759–780, https://doi.org/10.1038/NRD4593.

[3] J.T. Pedersen, N.H.H. Heegaard, Analysis of protein aggregation in neurodegenerative disease, Anal. Chem. 85 (2013) 4215–4227, https://doi.org/10.1021/AC400023C/ASSET/IMAGES/LARGE/AC-2013-00023C_0007.JPEG.

[4] M. Fujiwara, Z.K. Nagy, J.W. Chew, R.D. Braatz, First-principles and direct design approaches for the control of pharmaceutical crystallization, J. Process Control 15 (2005) 493–504, https://doi.org/10.1016/J.JPROCONT.2004.08.003.

[5] J.J. Roy, T.E. Abraham, Strategies in making cross-linked enzyme crystals, Chem. Rev. 104 (2004) 3705–3721, https://doi.org/10.1021/CR0204707/ASSET/IMAGES/LARGE/CR0204707F00005.JPEG.

[6] P.G. Vekilov, Dense liquid precursor for the nucleation of ordered solid phases from solution, Cryst. Growth Des. 4 (2004) 671–685, https://doi.org/10.1021/CG049977W/ASSET/IMAGES/LARGE/CG049977WF00018.JPEG.

[7] A.A. Jones, C.D. Snow, Porous protein crystals: synthesis and applications, Chem. Commun. 60 (2024) 5790–5803, https://doi.org/10.1039/D4CC00183D.

[8] F. Zhang, M.W.A. Skoda, R.M.J. Jacobs, R.A. Martin, C.M. Martin, F. Schreiber, Protein interactions studied by SAXS: effect of ionic strength and protein concentration for BSA in aqueous solutions, J. Phys. Chem. B 111 (2007) 251–259, https://doi.org/10.1021/JP0649955/ASSET/IMAGES/LARGE/JP0649955F00007.JPEG.

[9] S. Finet, F. Skouri-Panet, M. Casselyn, F. Bonneté, A. Tardieu, The Hofmeister effect as seen by SAXS in protein solutions, Curr. Opin. Colloid Interface Sci. 9 (2004) 112–116, https://doi.org/10.1016/J.COCIS.2004.05.014.

[10] L. Ianeselli, F. Zhang, M.W.A. Skoda, R.M.J. Jacobs, R.A. Martin, S. Callow, Sylvain Prévost, F. Schreiber, Protein-protein interactions in ovalbumin solutions studied by small-angle scattering: effect of ionic strength and the chemical nature of cations, (n.d.). doi: 10.1021/jp9112156.

[11] A. Ducruix, J.P. Guilloteau, M. Ri~s-Kautt, A. Tardieu, Protein interactions as seen by solution X-ray scattering prior to crystallogenesis, J. Cryst. Growth 168 (1996) 28–39.

[12] M.A. Haidekker, E.A. Theodorakis, Molecular rotors—fluorescent biosensors for viscosity and flow, Org. Biomol. Chem. 5 (2007) 1669–1678, https://doi.org/10.1039/B618415D.

[13] A.J. Thompson, T.W. Herling, M. Kubánková, A. Vyšniauskas, T.P.J. Knowles, M. K. Kuimova, Molecular rotors provide insights into microscopic structural changes during protein aggregation, J. Phys. Chem. B 119 (2015) 10170–10179, https://doi.org/10.1021/ACS.JPCB.5B05099/SUPPL_FILE/JP5B05099_SI_001.PDF.

[14] K. Suhling, P.M.W. French, D. Phillips, Time-resolved fluorescence microscopy, Photochem. Photobiol. Sci. 4 (2005) 13–22, https://doi.org/10.1039/B412924P.

[15] M.K. Kuimova, G. Yahioglu, J.A. Levitt, K. Suhling, Molecular rotor measures viscosity of live cells via fluorescence lifetime imaging, J. Am. Chem. Soc. 130 (2008) 6672–6673, https://doi.org/10.1021/JA800570D/SUPPL_FILE/JA800570D-FILE006.PDF.

[16] M.K. Kuimova, Mapping viscosity in cells using molecular rotors, PCCP 14 (2012) 12671–12686, https://doi.org/10.1039/C2CP41674C.

[17] I. López-Duarte, T. Truc Vu, M.A. Izquierdo, J.A. Bull, M.K. Kuimova, A molecular rotor for measuring viscosity in plasma membranes of live cells, Chem. Commun. 50 (2014) 5282–5284, https://doi.org/10.1039/C3CC47530A.

[18] L.E. Shimolina, M.A. Izquierdo, I. López-Duarte, J.A. Bull, M.V. Shirmanova, L. G. Klapshina, E.V. Zagaynova, M.K. Kuimova, Imaging tumor microscopic viscosity in vivo using molecular rotors, Sci. Reports 7 (2017) 1–11, https://doi.org/10.1038/srep41097.

[19] M. Kubánková, I. López-Duarte, J.A. Bull, D.M. Vadukul, L.C. Serpell, M. de Saint Victor, E. Stride, M.K. Kuimova, Probing supramolecular protein assembly using covalently attached fluorescent molecular rotors, Biomaterials 139 (2017) 195–201, https://doi.org/10.1016/J.BIOMATERIALS.2017.06.009.

[20] N.R. Anthony, A.K. Mehta, D.G. Lynn, K.M. Berland, Mapping amyloid-β(16–22) nucleation pathways using fluorescence lifetime imaging microscopy, Soft Matter 10 (2014) 4162–4172, https://doi.org/10.1039/C4SM00361F.

[21] S. Najafi, Y. Lin, A.P. Longhini, X. Zhang, K.T. Delaney, K.S. Kosik, G. H. Fredrickson, J.E. Shea, S. Han, Liquid–liquid phase separation of Tau by self and complex coacervation, Protein Sci. 30 (2021) 1393–1407, https://doi.org/10.1002/PRO.4101.

[22] W.L. Goh, M.Y. Lee, T.L. Joseph, S.T. Quah, C.J. Brown, C. Verma, S. Brenner, F. J. Ghadessy, Y.N. Teo, Molecular rotors as conditionally fluorescent labels for rapid detection of biomolecular interactions, J. Am. Chem. Soc. 136 (2014), https://doi.org/10.1021/ja413031h.

[23] A.S. Klymchenko, Y. Mely, Fluorescent environment-sensitive dyes as reporters of biomolecular interactions, Prog. Mol. Biol. Transl. Sci. 113 (2013) 35–58, https://doi.org/10.1016/B978-0-12-386932-6.00002-8.

[24] M. Schäferling, S. Nagl, Förster resonance energy transfer methods for quantification of protein-protein interactions on microarrays, Methods Mol. Biol. 723 (2011) 303–320, https://doi.org/10.1007/978-1-61779-043-0_19/COVER.

[25] P. Skehan, R. Storeng, D. Scudiero, A. Monks, J. Mcmahon, D. Vistica, J.T. Warren, H. Bokesch, S. Kenney, M.R. Boyd, New colorimetric cytotoxicity assay for anticancer-drug screening, J. Natl Cancer Inst. 82 (1990) 1107–1112, https://doi.org/10.1093/JNCI/82.13.1107.

[26] A. Vyšniauskas, M. Qurashi, N. Gallop, M. Balaz, H.L. Anderson, M.K. Kuimova, Unravelling the effect of temperature on viscosity-sensitive fluorescent molecular rotors, Chem. Sci. 6 (2015) 5773–5778, https://doi.org/10.1039/C5SC02248G.

[27] R. Franke, G.A. Holst, Frequency-domain fluorescence lifetime imaging system (pco.flim) based on a in-pixel dual tap control CMOS image sensor, Imaging,

Manipul., Analy. Biomol., Cells, Tissues XIII 9328 (2015) 93281K. doi: 10.1117/12.2087589.
[28] A.H.A. Clayton, Frequency-domain fluorescence lifetime imaging microscopy (FD-FLIM), in: Fluorescence practical manual for microscopy techniques, 2016, p. 12. https://www.picoquant.com/scientific/practical-manual-for-fluorescence-microscopy (accessed January 16, 2024).
[29] R. Datta, T.M. Heaster, J.T. Sharick, A.A. Gillette, M.C. Skala, Fluorescence lifetime imaging microscopy: fundamentals and advances in instrumentation, analysis, and applications, J. Biomed. Opt. 25 (2020) 1, https://doi.org/10.1117/1.JBO.25.7.071203.
[30] S. Monaco, E. Gordon, M.W. Bowler, S. Delagenière, M. Guijarro, D. Spruce, O. Svensson, S.M. Mcsweeney, A.A. Mccarthy, G. Leonard, M.H. Nanao, Automatic processing of macromolecular crystallography X-ray diffraction data at the ESRF, Urn:Issn:0021-8898 46 (2013) 804–810. doi: 10.1107/S0021889813006195.
[31] S. Basu, J.W. Kaminski, E. Panepucci, C.Y. Huang, R. Warshamanage, M. Wang, J. A. Wojdyla, Automated data collection and real-time data analysis suite for serial synchrotron crystallography, J. Synchrotron Radiat. 26 (2019) 244–252, https://doi.org/10.1107/S1600577518016570.
[32] M.D. Winn, C.C. Ballard, K.D. Cowtan, E.J. Dodson, P. Emsley, P.R. Evans, R. M. Keegan, E.B. Krissinel, A.G.W. Leslie, A. McCoy, S.J. McNicholas, G. N. Murshudov, N.S. Pannu, E.A. Potterton, H.R. Powell, R.J. Read, A. Vagin, K. S. Wilson, Overview of the CCP4 suite and current developments, Acta Crystallogr. D Biol. Crystallogr. 67 (2011) 235–242, https://doi.org/10.1107/S0907444910045749.
[33] A. Vagin, A. Teplyakov, Molecular replacement with MOLREP, Acta Crystallogr. D Biol. Crystallogr. 66 (2010) 22–25, https://doi.org/10.1107/S0907444909042589.
[34] G.N. Murshudov, P. Skubák, A.A. Lebedev, N.S. Pannu, R.A. Steiner, R.A. Nicholls, M.D. Winn, F. Long, A.A. Vagin, REFMAC5 for the refinement of macromolecular crystal structures, Acta Crystallogr. D Biol. Crystallogr. 67 (2011) 355–367, https://doi.org/10.1107/S0907444911001314.
[35] P. Emsley, B. Lohkamp, W.G. Scott, K. Cowtan, Features and development of Coot, Urn:Issn:0907-4449 66 (2010) 486–501. doi: 10.1107/S0907444910007493.
[36] J.B. Segur, H.E. Oderstar, Viscosity of glycerol and its aqueous solutions, Ind. Eng. Chem. 43 (1951) 2117–2120, https://doi.org/10.1021/IE50501A040/ASSET/IE50501A040.FP.PNG_V03.
[37] A. Vyšniauskas, M. Qurashi, N. Gallop, M. Balaz, H.L. Anderson, M.K. Kuimova, Unravelling the effect of temperature on viscosity-sensitive fluorescent molecular rotors, (2015). doi: 10.1039/c5sc02248g.
[38] W.J. Fredericks, M.C. Hammonds, S.B. Howard, F. Rosenberger, Density, thermal expansivity, viscosity and refractive index of lysozyme solutions at crystal growth concentrations, J. Cryst. Growth 141 (1994) 183–192, https://doi.org/10.1016/0022-0248(94)90111-2.
[39] R. Mercadé-Prieto, L. Rodriguez-Rivera, X.D. Chen, Fluorescence lifetime of Rhodamine B in aqueous solutions of polysaccharides and proteins as a function of viscosity and temperature, Photochem. Photobiol. Sci. 16 (2017) 1727–1734, https://doi.org/10.1039/C7PP00330G.
[40] E.L. Forsythe, R.A. Judge, M.L. Pusey, Tetragonal chicken egg white lysozyme solubility in sodium chloride, Solutions (1999), https://doi.org/10.1021/je980316a.
[41] M.M. Ries-Kautt, A.F. Ducruix, Relative effectiveness of various ions on the solubility and crystal growth of lysozyme, J. Biol. Chem. 264 (1989) 745–748, https://doi.org/10.1016/S0021-9258(19)85005-6.
[42] J.P. Guilloteau, M.M. Riès-Kautt, A.F. Ducruix, Variation of lysozyme solubility as a function of temperature in the presence of organic and inorganic salts, J. Cryst. Growth 122 (1992) 223–230, https://doi.org/10.1016/0022-0248(92)90249-I.
[43] P.D. Ross, S. Subramanian, Thermodynamics of protein association reactions: forces contributing to stability, Biochemistry 20 (1981) 3096–3102, https://doi.org/10.1021/BI00514A017/ASSET/BI00514A017.FP.PNG_V03.
[44] H. Rao, W. Qi, R. Su, Z. He, X. Peng, Mechanistic and conformational studies on the interaction of human serum albumin with rhodamine B by NMR, spectroscopic and molecular modeling methods, J. Mol. Liq. 316 (2020) 113889, https://doi.org/10.1016/J.MOLLIQ.2020.113889.
[45] S. Millan, L. Satish, S. Kesh, Y.S. Chaudhary, H. Sahoo, Interaction of Lysozyme with Rhodamine B: a combined analysis of spectroscopic & molecular docking, J. Photochem. Photobiol. B 162 (2016) 248–257, https://doi.org/10.1016/J.JPHOTOBIOL.2016.06.047.
[46] M. Kitamura, K. Murakami, K. Yamada, K. Kawai, M. Kunishima, Binding of sulforhodamine B to human serum albumin: a spectroscopic study, Dyes Pigm. 99 (2013) 588–593, https://doi.org/10.1016/J.DYEPIG.2013.06.011.
[47] P. Qin, B. Su, R. Liu, Probing the binding of two fluoroquinolones to lysozyme: a combined spectroscopic and docking study, Mol. Biosyst. 8 (2012) 1222–1229, https://doi.org/10.1039/C2MB05423J.
[48] N. Shahabadi, M. Maghsudi, S. Rouhani, Study on the interaction of food colourant quinoline yellow with bovine serum albumin by spectroscopic techniques, Food Chem. 135 (2012) 1836–1841, https://doi.org/10.1016/J.FOODCHEM.2012.06.095.
[49] S. Millan, L. Satish, K. Bera, B. Susrisweta, D.V. Singh, H. Sahoo, A spectroscopic and molecular simulation approach toward the binding affinity between lysozyme and phenazinium dyes: an effect on protein conformation, J. Phys. Chem. B 121 (2017) 1475–1484, https://doi.org/10.1021/ACS.JPCB.6B10991/ASSET/IMAGES/LARGE/JP-2016-109914_0008.JPEG.
[50] X. Mu, Z. Huang, W. Feng, M. Zhai, Y. Wang, D. Zhou, X. Zhou, Zwitterionic rhodamine-CPT prodrug nanoparticles with GSH/H2O2 responsiveness for cancer theranostics, Theranostics 13 (2023) 267, https://doi.org/10.7150/THNO.78884.
[51] J. Poznański, NMR-based localization of ions involved in salting out of hen egg white lysozyme, Acta Biochim. Pol. 53 (2006) 421–424, https://doi.org/10.18388/abp.2006_3357.